Critical Equivalent Series Resistance Estimation for Voltage Regulator Stability Using Hybrid System Identification and Neural Network

Mohd Hairi Mohd Zaman, M Marzuki Mustafa, Aini Hussain

Department of Electrical, Electronic and Systems Engineering, Universiti Kebangsaan Malaysia, 43600 Bangi, Selangor, Malaysia
E-mail: hairizaman@ukm.edu.my; marzuki@ukm.edu.my; draini@ukm.edu.my

Abstract— **Output capacitor in the voltage regulator (VR) circuit ensures stability especially during fast load transients. However, the capacitor parasitic, namely equivalent series resistance (ESR), may cause unstable VR operation. VR characterization in terms of ESR suggests stable range of capacitor ESR based on the ESR tunnel graph in the VR datasheet. Specifically, the stable ESR range is the critical ESR value, which lies on the failure region boundary of ESR tunnel graph. New or updated ESR tunnel graph through characterization is required for new product development or quality assurance purpose. However, the characterization is typically conducted manually in industry, thereby increases the manufacturing time and cost. Therefore, this work proposed a characterization approach that can reduce the time to determine the ESR tunnel graph based on the hybrid system identification and neural network (SI-NN) approach. This method utilised system identification (SI) to estimate the VR circuit model for certain operating points before predicting the transfer function coefficients for the remaining points using radial basis function neural network (RBFNN). Eventually, the critical ESR of failure region boundary was estimated. This hybrid SI-NN approach able to reduce the number of data that would be acquired manually to 25% compared to manual characterization, while provides critical ESR estimation with error less than 2%.**

Keywords— **Voltage regulator; output capacitor; equivalent series resistance; failure region boundary; system identification; radial basis function neural network.**

I. INTRODUCTION

Voltage regulator (VR) circuits with additional output capacitor are widely used in many electronic systems. VR converts the noisy and unstable voltage and current input supply to a stable, constant, accurate, and load-independent output supply [1]. VR has received much attention recently, mainly low dropout voltage type VR, due to the emerging market of new applications such as system-on-chip and Internet-of-Things, which require tight power consumption specification with stable and lower output voltages [2]–[4]. An output capacitor is connected to the VR output terminal to ensure stability.

Output capacitor in the VR circuit acts as a temporary energy storage component to compensate any instability especially during fast load transients [1], [5], [6]. Nowadays, many electronic systems include a lot of high speed digital signal processing. This high speed requirement requires fast load switching and transients. In this case, VR must be able to supply stable output voltage and current to the loads during those conditions.

However, the feedback mechanism inside the VR needs a minimum delay period to regulate its output. Therefore, once the load transient condition occurred, the output capacitor supplies temporary energy to the loads before the VR feedback able to regulate the VR output. This mechanism can be achieved only if the capacitor has optimum internal parasitic value [7], [8]. This capacitor parasitic is called equivalent series resistance (ESR).

Optimum capacitor's ESR compensates the VR instability before the internal VR feedback mechanism properly regulates the VR output. The ESR value compensates the feedback control loop in the power converter circuit such as VR by adding a zero in its transfer function. However, variations in age and temperature increase the ESR [9], [10]. Too high or too low ESR value may produce VR output with unreliable phase margin and eventually cause output oscillation and instability.

Therefore, VR manufacturers provides the stable ESR range in a special graph called ESR tunnel graph in their datasheet [1]. This type of graph shows the ESR versus load or output current plot for particular capacitance value. Fig. **1** shows an example of ESR tunnel graph for a commercial VR, model TPS76301 from Texas Instruments [11]. In this example, compensation series resistance, CSR is used instead of ESR, though it has the same function. For instance, the stable ESR range is located between 0.3 to 10 Ω, for load current from 50 to 250 mA. The ESR tunnel graph indicates

the passing and failure (or instability) regions, where the critical ESR lies on its failure region boundary.
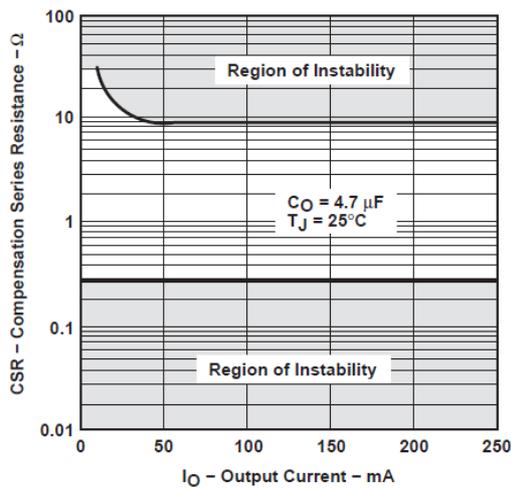

Fig. 1 Example of ESR tunnel graph for VR model TPS76301 from Texas Instruments (Source: Texas Instruments)

However, in practice, VR manufacturers manually perform VR characterization in terms of ESR by conducting time consuming tests on a range of ESR for different load currents [12]. Even though VR design phase normally considers the optimum ESR through the stability analysis of VR output dynamic or transient behaviour in terms of ESR effect [3], [13], actual VR performance varies for each unit of manufactured VR due to manufacturing process variation [12]. Detail VR internal circuit with actual component values and process variation parameters are required to analyse the stable ESR range of actual manufactured VR. Thus, exact model for actual VR sample is difficult to obtain for post analysis purpose. Hence, the manual VR characterization observes and analyses the actual dynamic or transient behaviour of manufactured VR samples and simultaneously plot the stability condition on the ESR tunnel graph for each operating point. Then, failure region boundary separating the stability and instability regions can be extracted from the graph. Eventually, the critical ESR lies on the failure region boundaries can be determined.

Since the manual characterization consumes a lot of time and cost, there is a need to improve the characterization process. At the same time, the improved characterization method must be able to produce reliable results. Since VR circuit is an analog circuit, therefore, this issue can be categorized as an analog circuit test and analysis issue. Much research have been done to test and analyse the analog circuit without knowing the exact model of the circuit under test, such as through transfer coefficient based [14]–[16] and black-box modelling [17]. Some work also have been conducted to estimate the failure region boundary of analog circuit [18]–[20]. In addition, most research on capacitor ESR only concentrates for the purpose of condition monitoring and fault diagnosis [21]–[23]. However, not much research has been done on the testing and characterization in terms of capacitor ESR for power converter packaged in integrated circuit form such as voltage regulator.

Therefore, this paper improves the VR characterization process by applying hybrid approach of system identification (SI) and neural network (NN), in short SI-NN. In particular, the critical ESR values located on the failure region boundaries of ESR tunnel graph are determined using this hybrid SI-NN-based characterization and finally compared with the manual characterization outcome.

II. MATERIAL AND METHOD

The hybrid SI-NN-based VR characterization proposed in this work estimates the VR circuit model using system identification for a number of operating points and then predicting the VR circuit transfer function coefficients based on the trained radial basis function neural network (RBFNN). The proposed method performance was compared with the benchmark extracted from manual characterization. Fig. 2 depicts the overall process flow in SI-NN-based characterization starting from manual characterization, failure region boundary benchmark search, VR circuit model modelling through SI, dataset reduction, RBFNN training, transfer function coefficients prediction using trained RBFNN, failure region boundary estimation, and finally validation. Before describing the individual process in detail, the VR selection and test circuit development will be elaborated first.
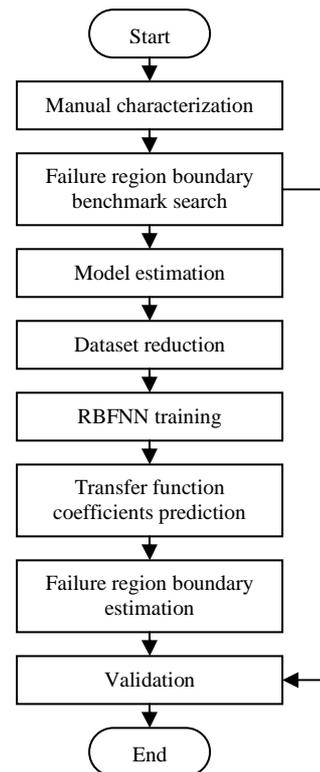

Fig. 2 Flowchart of the hybrid SI-NN-based VR characterization

A. VR Selection

In this work, VR model series TPS763XX, manufactured by Texas Instruments was selected because its datasheet is more comprehensive indicating two ESR tunnel graphs for two different output capacitor's capacitance [11]. Furthermore, the ESR tunnel graph of this VR model has three regions as shown in Fig. 1, where the stable region is

located in between two failure or instability regions. So, there are two failure region boundaries which indicates that the ESR value cannot be too low or too high. Some ESR tunnel graphs from another VR manufacturers only have single failure region boundary. Meanwhile, some manufacturers only state the stable ESR range without showing any ESR tunnel graph in their datasheet [24].

B. Test Circuit Development

TPS763XX series VR has various models, differentiated by the output voltage. The specific VR model selected in this work was TPS76301 which is an adjustable-type VR. So, different output voltages can be tested using single VR. To set the output voltage, for instance 5 V, resistance of two resistors, R_1 and R_2, need to be configured to 549 and 169 kΩ, respectively, as shown in the test circuit in Fig. 3. The test circuit includes a resistor, R_{ESR}, connected in series with the output capacitor, C_{out}. In real circuit, R_{ESR} can be a combination of the internal ESR of C_{out} and additional compensation series resistor. There is also a signal generator, V_s, that disturbs the load current when its level is changed.
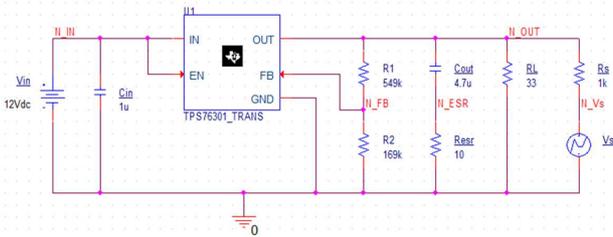

Fig. 3 TPS76301 test circuit

C. Manual VR Characterization

After selecting the suitable VR model and constructing the test circuit, manual VR characterization was conducted. The manual characterization purpose is to find the failure region boundary benchmark for each load current. In this work, the load current range is between 50 to 150 mA with 25 mA increment, meanwhile the ESR range is from 0.1 to 15 Ω with 0.1 Ω increment. Each combination of ESR and load current represents an operating point in the ESR tunnel graph. Initial ESR and load current were configured as equal to corresponding minimum values. Manual characterization was executed until all operating points have been characterized.

For each operating point, following processes were conducted in manual characterization. The first process was to initialize the input voltage, load current and ESR. Simultaneously, the start time of characterization was recorded. Then the test circuit was simulated in OrCAD with specific ESR and load current. In this case, the OrCAD simulation was fully controlled by MATLAB. Particularly, MATLAB generated the circuit netlist file in a text file format before executing the OrCAD simulation. This circuit netlist file contains all circuit configurations such as the nodes, connection and component values. After the circuit simulation has been successfully executed, MATLAB imported the circuit raw data file for further analysis.

The subsequent process analysed the VR dynamic behaviour in terms of load transient response. During circuit simulation, after specific delay, for example 1.5 s, the load

current was disturbed. In detail, the output voltage level of signal generator, V_s, as shown in Fig. 3, was changed abruptly, firstly from low to high level, and then from high to low level. After that, undershoot and overshoot voltages of VR output were computed. The undershoot voltage is the difference between initial and minimum VR output voltage. Meanwhile, the difference between maximum and initial VR output voltage is called overshoot voltage. Both undershoot and overshoot voltages are the main parameters for VR stability judgment.

The final process in the manual characterization is to determine whether the VR is stable or not. In this work, the stable ESR range from the VR datasheet was used as reference. The datasheet states that in order to guarantee VR stability, the ESR value must be between 0.3 to 10 Ω. The corresponding undershoot and overshoot voltages related to this stable ESR range act as the specification during stability determination for another operating points [25], [5]. For example, for load current of 50 mA and ESR of 0.3 Ω, the undershoot and overshoot voltages are US_1 and $OS1_1$ V, accordingly. In the meantime, US_2 and OS_2 V are the undershoot and overshoot voltages when the ESR is equal to 10 Ω. Therefore, for each operating point, if the measured undershoot is within US_1 and US_2, and the measured overshoot is between OS_1 and OS_2, then the VR is judged as stable. Otherwise, the VR is considered as unstable. Finally, the ESR tunnel graph was plotted for all operating points, i.e. all load currents and ESR values, with corresponding stability condition.

D. Failure Region Boundary Benchmark Search

The failure region boundary benchmark was obtained from the plotted ESR tunnel graph. The failure region boundary is defined as the ESR values separating the stable (passing) and unstable (failure) regions in the ESR tunnel graph. For each load current in the manual characterization, the failure region boundary was analysed and then became as the benchmark for later SI-NN-based VR characterization.

E. VR Model Estimation Using SI

Hybrid SI-NN-based VR characterization begins with the VR circuit model estimation by applying SI method. SI method is widely utilized to estimate the unknown system model, provided input and output data are available. Input and output data in this work were disturbance voltage, V_s and output voltage, V_{out} respectively. Model estimated using SI method typically has gone through several procedures starting from preprocessing, data division, model structure selection, model estimation and finally model validation.

Firstly, preprocessing procedure removed the mean values from both input and output data. Then, the input and output data was divided into estimation and validation data. Half of the data was allocated as the estimation data while the rest was for validation purpose.

The following process is to select the suitable model structure that able to represent the VR circuit. Model structure is the mathematical expression that relates the input and output variables. This model structure consists of unknown model parameters that need to be estimated. Typical model structures available in SI are Autoregressive with Exogenous Input (ARX), Output Error (OE),

Autoregressive Moving Average with Exogenous Input (ARMAX) and Box-Jenkins (BJ) model structures. OE model structure was chosen in this work because it has less number of model parameters compared with other model structures. Equation (1) describes the OE model structure equation,

$$y(k) = \frac{B(q)}{F(q)} u(k - n_k) + e(k) \qquad (1)$$

where y and u are the input and output respectively, while $e(k)$ is the white noise with zero mean, and n_k is the number of delay, with k is the sample instant. Furthermore, polynomial $B(q)$ and $F(q)$ can be described in terms of backward shift operator, q as stated in (2) and (3) as follows,

$$B(q) = b_1 + b_2 q^{-1} + \cdots + b_{n_b} q^{-n_b+1} \qquad (2)$$

$$F(q) = 1 + f_1 q^{-1} + \cdots + f_{n_f} q^{-n_f} \qquad (3)$$

with n_b is the order of polynomial $B(q)$ and n_f is the order of polynomial $F(q)$.

The subsequent process is the model estimation. This process, which can be analysed as a least square problem for linear regression, can be written as,

$$y(k, \theta) = \Phi(k)^T \theta = \xi(k, \theta) \qquad (4)$$

with the regressor vector, $\Phi(k)$, can be defined as,

$$\begin{aligned} \Phi(k) = [&u(k-1), u(k-2), \ldots, u(k-n_b), \\ &-\xi(k-1,\theta), -\xi(k-2,\theta), \ldots, -\xi(k-n_f, \theta)] \end{aligned} \qquad (5)$$

Meanwhile, the parameter vector, θ, which consists of unknown model parameters or transfer function coefficients, can be stated as,

$$\theta = [b_1, b_2, \cdots, b_{n_b}, f_1, f_2, \cdots, f_{n_f}]^T \qquad (6)$$

In detail, the model estimation estimates the parameter vector, θ by minimizing the error between the estimated model output and actual measured output data through the cost function manipulation. The best estimate of parameter vector was obtained when the cost function was minimum.

After the VR circuit model has been estimated, the model need to be validated. Therefore, the validation data was applied to the estimated model, in particular, the estimated transfer function. Then, the model fitness was computed. In this work, the model was simulated by applying two types of step signals to obtain the transient responses. The first step signal was executed when changing V_s level from 2 to 5V, whereas the second step signal changed the V_s level from 5 to 2 V. In addition, the optimum n_b, n_f and n_k configuration were defined after conducting iterative search and then evaluating the model fitness when applying the validation data.

Further processes have been conducted to obtain the ESR tunnel graph based on the transient response from the prior estimated model simulation. As in the manual characterization, undershoot and overshoot voltages were also computed from those transient responses. Then, VR stability was determined for each operating point before plotting the ESR tunnel graph. At this stage, a dataset comprises of transfer function coefficients based on the estimated model using SI for all operating points was completely developed.

F. Dataset Reduction

The next stage was to train the RBFNN structure before it can be used for transfer function coefficients prediction. Before training the RBFNN structure, the SI-based dataset need to be reduced first. This dataset reduction purpose is to reduce the number of operating points that need to be manually acquired, so eventually it will reduce the VR characterization time. In detail, the dataset was reduced based on a dataset reduction factor. For example, initial configuration of ESR range was from 0.1 to 15 Ω with increment step of 0.1 Ω producing total 150 ESR values. If the dataset reduction factor was configured to 2, the next ESR was the next two ESR value from the current ESR. In this case, the ESR was skipped one point. Therefore, the ESR range of the reduced dataset was configured from 0.1 to 14.9 Ω with 0.2 Ω increment step. The new dataset then contains only 75 ESR values, which was 50% reduced compared to the original manual characterization dataset.

G. RBFNN Training

As mentioned earlier, the SI-NN-based VR characterization in this work predicted the transfer function coefficients after estimating the VR circuit model, which can be viewed as a function approximation or regression problem. Other research uses optimization approach to select the optimal SI model structure [26]. RBFNN has been chosen since its structure is simpler than another type of neural network such as multilayer perceptron neural network.

RBFNN structure basically contains input, hidden and output layers as depicted in Figure 4. The input layer receives the external input signals and redistributes these signals to the hidden layer. The hidden layer has neurons or nodes with radial basis function. Commonly used radial basis function is Gaussian function described as follows,

$$\varphi(x, \mu) = e^{\frac{\|x - \mu\|^2}{2d^2}} \qquad (7)$$

where x is the input, μ is the mean or centre of x and d is the distance from the centre of $\varphi(x, \mu)$ to the outer of Gaussian bell curve which also represents the spread of the Gaussian function. So, two important parameters are associated to these RBFNN neurons, which related to the Gaussian function properties, namely the centre, μ and spread, d. The Gaussian function indicates that the hidden neuron sensitivity can be adjusted by manipulating the d parameter. This means that the hidden neurons are more sensitive to the data points towards the centre of the Gaussian curve. In addition, the radial basis function is also widely used in other machine learning algorithm such as in support vector

machine [27]. Lastly, the output layer produces a weighted sum of its input taken from the output of hidden layer.
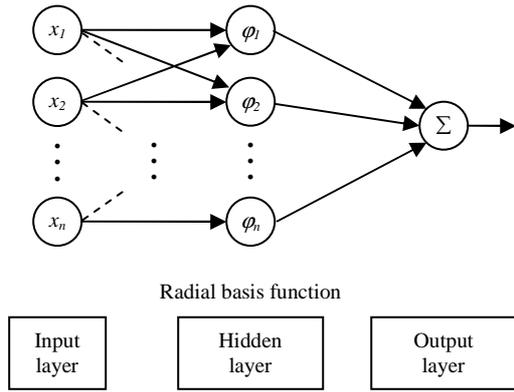

Fig. 4 RBFNN structure

In this work, the RBFNN structure was trained with ESR and initial load current as the inputs, while individual transfer function coefficients as the outputs. ESR and initial load current were selected as the RBFNN inputs because each operating point in the ESR tunnel graph must has these two variables. ESR was not selected as the RBFNN output, even though the main aim of this work is to estimate the critical ESR. The critical ESR can only be estimated after plotting the stability condition for all operating points in the ESR tunnel graph. In order to obtain the stability condition, transient response need to be simulated first using the transfer function. Therefore, the individual transfer function coefficients were selected as RBFNN outputs. Each transfer function coefficient in (2) and (3) was configured in individual RBFNN structure, as depicted in Fig. 5. For example, if the SI-estimated VR model has six transfer function coefficients consists of two poles and four zeros, then there will be six RBFNN structures need to be trained. The network was trained until convergence, which is until the training mean squared error (MSE) has met its goal, for instance, MSE should be nearly zero. On the other hand, this work also analysed the best spread of the Gaussian function. After completing the training process, the RBFNN structure was available for subsequent transfer function coefficient prediction process.
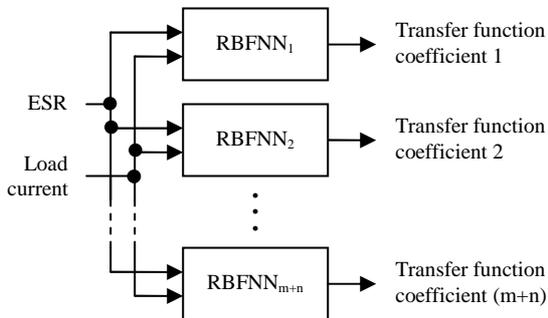

Fig. 5 Individual RBFNN structure for each transfer function coefficient

H. Transfer Function Coefficients Prediction

The trained RBFNN was then used for predicting the transfer function coefficients for all operating points same as

in the manual VR characterization, which were not included in the training dataset. Each transfer function coefficient was predicted independently since it was trained individually. Then, all predicted transfer function coefficients were combined in the transfer function form, same as the estimated transfer function obtained in prior SI method.

After that, two step signals as used in the validation phase of SI method previously were applied to the transfer function that incorporates RBFNN-predicted coefficients for each operating point. The transient responses were obtained from the transfer function simulation. Then, from the transient responses, undershoot and overshoot voltages were measured. These voltages were evaluated whether the VR was in stable condition or not before plotting the ESR tunnel graph of SI-NN-based VR characterization.

I. Failure Region Boundary Estimation

Based on the ESR tunnel graph of SI-NN-based characterization, the critical ESR lies on the failure region boundary for each load current were estimated. Then, failure region boundary, together with passing and failure regions were estimated.

J. Validation

Finally, the critical ESR of estimated failure region boundary obtained from SI-NN-based characterization was compared with the benchmark from manual VR characterization. Five performance metrics were used in evaluating the predicted critical ESR values that lie on the failure region boundary, namely mean squared error (MSE), root mean squared error (RMSE), mean absolute error (MAE), correlation coefficient (R^2) and relative error (RE). Following equation (8) to (12) describe these performance metrics.

$$MSE = \frac{1}{N}\sum_{i=1}^{n}\left[y(i) - y_p(i)\right]^2 \tag{8}$$

$$RMSE = \sqrt{\frac{1}{N}\sum_{i=1}^{n}\left[y(i) - y_p(i)\right]^2} \tag{9}$$

$$MAE = \frac{1}{N}\sum_{i=1}^{n}\left|y(i) - y_p(i)\right| \tag{10}$$

$$R^2 = \frac{\sum_{i=1}^{n}\left[\left(y(i) - \overline{y}(i)\right)\left(y_p(i) - \overline{y}_p(i)\right)\right]}{\sqrt{\sum_{i=1}^{n}\left(y(i) - \overline{y}(i)\right)^2\sum_{i=1}^{n}\left(y_p(i) - \overline{y}_p(i)\right)^2}} \tag{11}$$

$$RE = \left(\frac{y(i) - y_p(i)}{y(i)}\right)100 \tag{12}$$

where y and y_p are the actual and predicted critical ESR corresponding to the failure region boundary, n is the number of observations and i is the load current instant. SI-NN-based characterization has better performance if MSE,

RMSE and MAE values are closer to zero. Meanwhile, the R^2 must closer to one to indicate that the SI-NN-based characterization has better performance. Lastly, RE is computed to measure the relative accuracy of the SI-NN-based characterization.

III. RESULTS AND DISCUSSION

A. Manual VR Characterization Results

The main aim of this work is to improve the VR characterization by providing reliable estimation of VR failure region boundary and its critical ESR. The improved method is only considered reliable if it is able to produce the critical ESR near or equals to the failure region boundary benchmark.

A benchmark based on the ESR tunnel graph of manual VR characterization was obtained as displayed in Fig. 6. Fig. 6(a) shows that there are three distinct regions, where the passing region (stable region) on the middle part of the graph resides between two failure regions (instability regions) at the lower and upper parts of the ESR tunnel graph. In addition, Fig. 6(b) which depicts a portion of the overall results, for load current of 50 mA and ESR from 9.8 to 10.1 Ω with 0.1 Ω increment, indicates clear boundaries between passing and failure regions. For each operating point, which is the pair of load current and ESR, the circle mark indicates the stable VR output, whereas the cross mark represents VR instability. Therefore, there are two failure region boundaries, namely upper and lower boundaries. These boundaries are the benchmark for SI-NN-based characterization later.
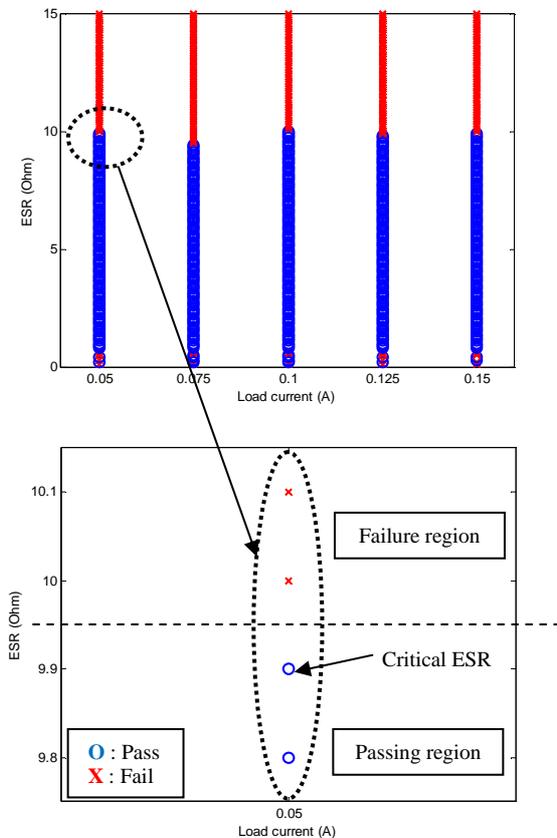

Fig. 6 ESR tunnel graph of manual VR characterization acts as benchmark (a) All results (b) A portion of the overall results

B. SI-NN-Based VR Characterization Results

Once the failure region boundaries benchmark has been defined, the SI-NN-based VR characterization was conducted. The VR circuit transfer function coefficients were predicted using trained RBFNN structure including the operating points that have been removed during SI-based dataset reduction stage. Fig. 7 displays the ESR tunnel graph of SI-NN-based characterization as proposed in this work with optimum SI and NN configuration. It can be seen that there are also three distinct regions similar as manual characterization result. Meanwhile, Fig. 8 indicates that the critical ESR lies on the failure region boundaries of manual and SI-NN-based characterization are similar for each load current. This best SI-NN-based characterization result was obtained after selecting the best SI and NN configurations.

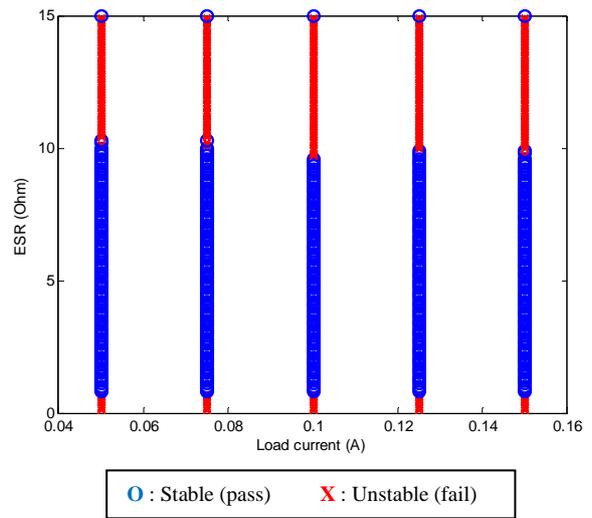O : Stable (pass)   X : Unstable (fail)

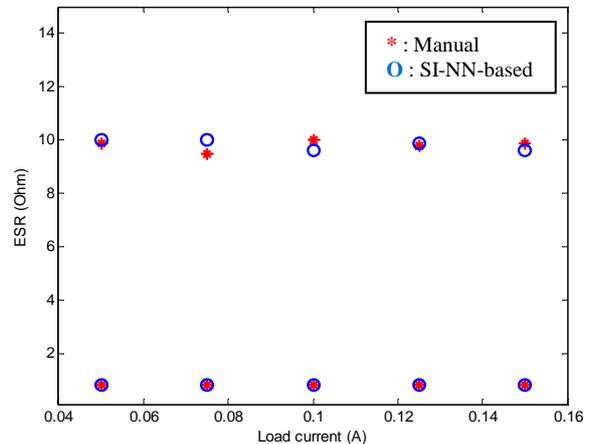Fig. 7 ESR tunnel graph of SI-NN-based VR characterization

Fig. 8 Comparison of critical ESR on the failure region boundaries between manual and SI-NN-based VR characterization

VR circuit model was estimated using SI with the best configurations including the best model structure and its order of polynomial. After iteratively testing various SI configurations, it was found that the best model structure was OE model with n_b, n_f and n_k set to 4, 2, and 0 accordingly. The best SI configuration was determined based on the highest model fitness percentage. The estimated models for all operating points using this best configuration

has fitness mean of 99.8%. Fig. 9 compares the transient responses from manual characterization and SI-estimated VR circuit model for ESR of 10 Ω and load current of 50 mA. At 2 s, the load current was changed abruptly and at the same time the output voltage was observed. Both overshoot voltages shown in Fig. 9 are similar, which indicates that the SI-estimated model was reliable.
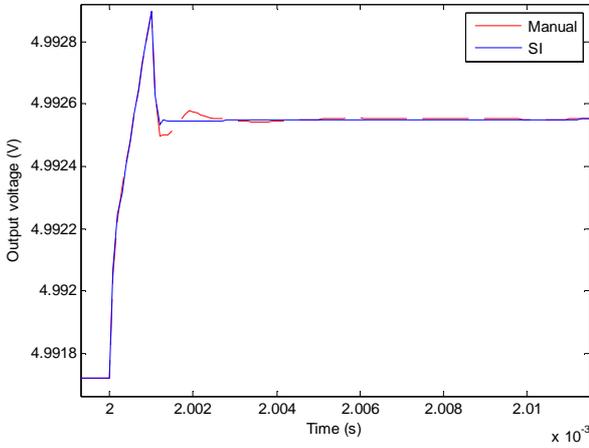

Fig. 9 Transient responses from manual characterization and SI-estimated model simulation for ESR of 10 Ω and load current of 50 mA

After obtaining the best SI configuration, the optimum RBFNN spread and maximum dataset reduction factor were analysed to find the best SI-NN-based characterization results. Fig. 10 shows that RBFNN spread less than 0.25 contributes high critical ESR prediction MSE. Furthermore, Table 1 depicts all computed performance metrics for different RBFNN spreads. It can be concluded that RBFNN spread of 0.25 yields the best performance with MSE, RMSE, MAE, R^2 and RE mean are 0.05, 0.23, 0.14, 0.9987 and 1.43, respectively.
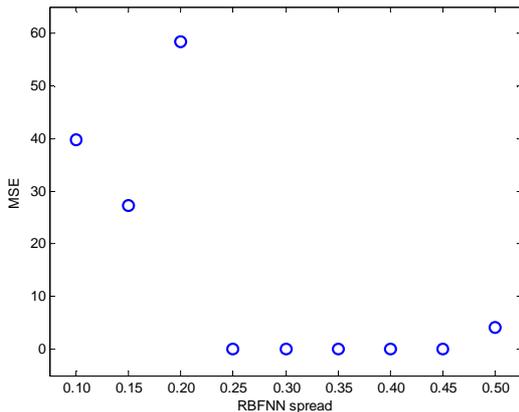

Fig. 10 MSE of critical ESR prediction on failure region boundary for various RBFNN spread

RBFNN spread	Performance metric				
	MSE	RMSE	MAE	R^2	RE
0.10	39.80	6.31	4.51	0.0000	51.67
0.15	27.34	5.23	3.61	0.3938	422.57
0.20	58.48	7.65	6.13	0.0795	547.97
0.25	**0.05**	**0.23**	**0.14**	**0.9987**	**1.43**
0.30	0.07	0.27	0.16	0.9984	1.63
0.35	0.07	0.27	0.16	0.9984	1.63
0.40	0.08	0.29	0.20	0.9983	5.48
0.45	0.08	0.27	0.19	0.9730	5.38
0.50	4.05	4.83	1.43	0.3788	166.12

In addition, the maximum dataset reduction factor was also determined. Fig. 11 shows the RE mean of critical ESR prediction for various dataset reduction factors. In this case, the RBFNN spread of 0.25 was applied. If the dataset reduction factor is greater than 4, then the RE mean becomes higher than 5% indicating unreliable results. So, the maximum reduction factor is 4 with RE mean of critical ESR prediction of 1.43%. In this work, the critical ESR prediction error was set to be less than 5%. This result concludes that even though the number of manually acquired data was reduced up to 75%, SI-NN-based VR characterization still be able to estimate reliable failure region boundary, which eventually will reduce the characterization time. The reduced dataset used to train the RBFNN structure was only 190 data points or 25% from the original 750 data points in the manual VR characterization.
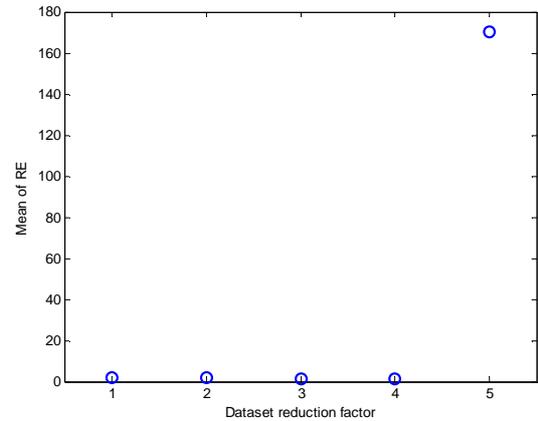

Fig. 11 MSE of critical ESR prediction on failure region boundary for different dataset reduction factors

IV. CONCLUSION

An improved VR characterization in terms of finding the critical ESR lying on the failure region boundary based on hybrid SI and RBFNN approach was investigated in this work. This work has developed a method that initially estimates the VR circuit model using SI method for reduced number of operating points and subsequently predicts the transfer function coefficients for the remaining operating points using RBFNN. In the end, the critical ESR value on the failure region boundary obtained from the improved SI-NN-based method was compared with the benchmark extracted from the manual VR characterization. The critical ESR comparison result shows good correlation. Furthermore, the result was achieved after describing the best

configuration of SI and RBFNN. In conclusion, hybrid SI-NN-based VR characterization has shortened the VR characterization process.

REFERENCES

[1] G. Rincon-Mora, "Analog IC Design with Low-Dropout Regulators (LDOs)," United States of America: McGraw-Hill, 2009.

[2] C. C. Bilberry, M. S. Mazzola, and J. Gafford, "Power supply on chip (PwrSoC) model identification using black-box modeling techniques," in *Proc. 2012 Twenty-Seventh Annual IEEE Applied Power Electronics Conference and Exposition (APEC 2012)*, 2012, pp. 1821–1825.

[3] T. Coulot, E. Lauga-Larroze, J. M. Fournier, M. Alamir, and F. Hasbani, "Stability analysis and design procedure of multiloop linear LDO regulators via state matrix decomposition," *IEEE Trans. Power Electron.*, vol. 28, no. 11, pp. 5352–5363, 2013.

[4] S. B. Nasir, S. Gangopadhyay, and A. Raychowdhury, "All-Digital Low-Dropout Regulator With Adaptive Control and Reduced Dynamic Stability for Digital Load Circuits," *IEEE Trans.Power Electron.*, vol. 31, no. 12. pp. 8293–8302, 2016.

[5] *Robust Dimensioning of the Output Capacitor: Application Note*, Infineon, 2014.

[6] *LDO Regulator Stability Using Ceramic Output Capacitors*, Texas Instruments, 2013.

[7] B. S. Lee, "Understanding the stable range of equivalent series resistance of an LDO regulator," *Analog Appl. J.*, no. November, pp. 14–17, 1999.

[8] S. Sandler. (2011) A simple method to determine ESR requirements for stable regulators. [Online]. Available: http://powerelectronics.com/power-management/simple-method-determine-esr-requirements-stable-regulators

[9] K. Harada, A. Katsuki, and M. Fujiwara, "Use of ESR for deterioration diagnosis of electrolytic capacitor," *IEEE Trans. Power Electron.*, vol. 8, no. 4, pp. 355–361, 1993.

[10] Y. Chen, H. Malek, and S. Dadras, "Fractional order equivalent series resistance modelling of electrolytic capacitor and fractional order failure prediction with application to predictive maintenance," *IET Power Electron.*, vol. 9, no. 8, pp. 1608–1613, 2016.

[11] "TPS76301, TPS76316, TPS76318, TPS76325, TPS76327, TPS76328, TPS76330, TPS76333, TPS76338, TPS76350 low-spower 150-mA low-dropout linear regulators data sheet," Texas Instruments, Texas, United States of America.

[12] A. H. Musa, M. H. M. Zaman, R. Mohamed, and M. M. Mustafa, "Characterization of voltage regulators by automated equivalent series resistance," in *Proc. IEEE Conference on Systems, Process and Control (ICSPC 2014)*, 2014, pp. 68–72.

[13] G. A. Rincon-Mora and P. E. Allen, "A low-voltage, low quiescent current, low drop-out regulator," *IEEE J. Solid-State Circuits*, vol. 33, no. 1, pp. 36–43, 1998.

[14] Z. Guo and J. Savir, "Coefficient-based test of parametric faults in analog circuits," *IEEE Trans. Instrum. Meas.*, vol. 55, no. 1, pp. 150–157, 2006.

[15] Z. Guo and J. Savir, "Analog circuit test using transfer function coefficient estimates," in *Proc. International Test Conference (ITC 2003)*, 2003, vol. 1, pp. 1155–1163.

[16] S. Sindia, V. Singh, and V. D. Agrawal, "Polynomial coefficient based DC testing of non-linear analog circuits," *Proc. 19th ACM Gt. Lakes Symp. VLSI (GLSVLSI '09)*, 2009, no. 3, pp. 69–74.

[17] T. Souvignet, T. Coulot, Y. David, S. Trochut, T. Di Gilio, and B. Allard, "Black box small-signal model of PMOS LDO voltage regulator," *Proc. 39th Annual Conference of the IEEE Industrial Electronics Society (IECON 2013)*. 2013. pp. 495–500.

[18] R. D. Amariutei, L. Goras, M. Dobler, M. Rafaila, A. Buzo, and G. Pelz, "On the stability domain of a DC-DC buck converter with software control loop," in *Proc. 19th International Conference on System Theory, Control and Computing (ICSTCC 2015)*, 2015, pp. 811–816.

[19] M. Dobler, M. Harrant, M. Rafaila, G. Pelz, W. Rosenstiel, and M. Bogdan, "Bordersearch: An adaptive identification of failure regions," in *Proc. 2015 Design, Automation & Test in Europe Conference & Exhibition (DATE 2015)*, 2015, no. 1, pp. 1036–1041.

[20] C. Grimm and C. Radojicic, "Verification and validation of AMS systems: Towards coverage of uncertainties," *Proc. 2015 IEEE 20th Int. Mix. Test Work (IMSTW 2015)*, 2015. pp. 1–6.

[21] A. V. T. Leite, H. J. A. Teixeira, A. J. M. Cardoso, and R. M. E. Araujo, "A simple ESR identification methodology for electrolytic capacitors condition monitoring," *Proc. 20th Congr. Cond. Monit. Diagnostic Eng. Manag.*, 2007, no. 2002, pp. 75–84.

[22] A. M. Imam, "Real-time condition monitoring of the electrolytic capacitors for power electronics applications," in *Proc. Twenty-Second Annual IEEE Applied Power Electronics Conference and Exposition*, 2007, pp. 1057–1061.

[23] H. Soliman, H. Wang, B. Gadalla, and F. Blaabjerg, "Condition monitoring for DC-link capacitors based on artificial neural network algorithm," in *Proc. 2015 IEEE 5th International Conference on Power Engineering, Energy and Electrical Drives (POWERENG 2015)*, 2015, pp. 587–591.

[24] "LT1963A series: 1.5A, low noise, fast transient response LDO regulators data sheet," California, United States of America.

[25] S. B. Nasir, S. Gangopadhyay, and A. Raychowdhury, "All-digital low-dropout regulator with adaptive control and reduced dynamic stability for digital load circuits," *IEEE Trans. Power Electron.*, vol. 31, no. 12. pp. 8293–8302, 2016.

[26] I. M. Yassin, A. Zabidi, M. S. A. M. Ali, N. M. Tahir, H. Z. Abidin, and Z. I. Rizman, "Binary particle swarm optimization structure selection of nonlinear autoregressive moving average with exogenous inputs (NARMAX) model of a flexible robot arm," *Int. J. Adv. Sci. Eng. Inf. Technol.*, vol. 6, no. 5, pp. 630–637, 2016.

[27] F. H. Anuwar and A. M. Omar, "Future Solar Irradiance Prediction using Least Square Support Vector Machine," *Int. J. Adv. Sci. Eng. Inf. Technol.*, vol. 6, no. 4, pp. 520–523, 2016.